


Article

Automatic Classification of Fatty Liver Disease Based on Supervised Learning and Genetic Algorithm

Ahmed Gaber ^{1,*}, Hassan A. Youness ¹, Alaa Hamdy ^{2,*}, Hammam M. Abdelaal ³ and Ammar M. Hassan ⁴ 

¹ Department of Computers & Systems Engineering, Faculty of Engineering, Minia University, Minia 61519, Egypt; hassan_youness@mu.edu.eg

² Department of Communications, Electronics, and Computer, Faculty of Engineering, Helwan University, Cairo 11511, Egypt

³ Department of Information Technology, Faculty of Computers and Information, Luxor University, Luxor 85951, Egypt; hammam_abdelaal@fci.luxor.edu.eg

⁴ Arab Academy for Science, Technology and Maritime Transport, South Valley Branch, Aswan 81516, Egypt; ammar@aast.edu

* Correspondence: agaber2008@csi.edu.eg (A.G.); alaa.hamdy@h-eng.helwan.edu.eg (A.H.)

Abstract: Fatty liver disease is considered a critical illness that should be diagnosed and detected at an early stage. In advanced stages, liver cancer or cirrhosis arise, and to identify this disease, radiologists commonly use ultrasound images. However, because of their low quality, radiologists found it challenging to recognize this disease using ultrasonic images. To avoid this problem, a Computer-Aided Diagnosis technique is developed in the current study, using Machine Learning Algorithms and a voting-based classifier to categorize liver tissues as being fatty or normal, based on extracting ultrasound image features and a voting-based classifier. Four main contributions are provided by our developed method: firstly, the classification of liver images is achieved as normal or fatty without a segmentation phase. Secondly, compared to our proposed work, the dataset in previous works was insufficient. A combination of 26 features is the third contribution. Based on the proposed methods, the extracted features are Gray-Level Co-Occurrence Matrix (GLCM) and First-Order Statistics (FOS). The fourth contribution is the voting classifier used to determine the liver tissue type. Several trials have been performed by examining the voting-based classifier and J48 algorithm on a dataset. The obtained TP, TN, FP, and FN were 94.28%, 97.14%, 5.71%, and 2.85%, respectively. The achieved precision, sensitivity, specificity, and F1-score were 94.28%, 97.05%, 94.44%, and 95.64%, respectively. The achieved classification accuracy using a voting-based classifier was 95.71% and in the case of using the J48 algorithm was 93.12%. The proposed work achieved a high performance compared with the research works.



Citation: Gaber, A.; Youness, H.A.; Hamdy, A.; Abdelaal, H.M.; Hassan, A.M. Automatic Classification of Fatty Liver Disease Based on Supervised Learning and Genetic Algorithm. *Appl. Sci.* **2022**, *12*, 521. <https://doi.org/10.3390/app12010521>

Academic Editor: Francisco Arrebola

Received: 14 November 2021

Accepted: 30 December 2021

Published: 5 January 2022

Publisher's Note: MDPI stays neutral with regard to jurisdictional claims in published maps and institutional affiliations.



Copyright: © 2022 by the authors. Licensee MDPI, Basel, Switzerland. This article is an open access article distributed under the terms and conditions of the Creative Commons Attribution (CC BY) license (<https://creativecommons.org/licenses/by/4.0/>).

Keywords: Computer-Aided Diagnosis; diffuse liver; fatty liver; feature extraction; region of interest; voting-based classifier; learning algorithms; ultrasound

1. Introduction

Diffuse liver conditions, including fatty liver, are the world's leading cause of death [1], and Fatty Liver Disease (FLD) has a prevalence of 25 percent worldwide. Nonalcoholic Liver Fatty Disease (NALFD) and its subtype, nonalcoholic steatohepatitis, affect 30 percent and 5 percent of people in the USA, respectively [2]. Asia and Africa were found to have the most observed prevalence of FLD [3]. There are several categories of hepatic disorders; those caused by poisons, too much alcohol, or drugs. Other kinds of diseases are caused by viruses, such as hepatitis B and C.

Liver diseases can be caused by many other factors, including high blood sugar, insulin resistance, and obesity. Fatty liver can be treated if it is possibly identified at an early stage, a changeable condition, which is categorized by the accumulation of liver fat, and this deposition can be due to nonalcoholic origin or excessive consumption of alcohol. FLD is

associated with several features such as insulin resistance, diabetes, hyperlipidemia, and viral hepatitis [4].

2. Background

FLD may progress to advanced liver diseases, such as hepatic transaminases, cryptogenic hepatocellular disease, and cirrhosis, which may eventually result in death [5,6]. Table 1 shows the ultrasound (US) findings and specific causes of liver disease. Despite the accurate results of liver biopsy for FLD detection and diagnosis; however, it has certain associated weaknesses. Those weaknesses consist of bleeding until death, penetration of the skin, and some complications, e.g., increased abdominal pain, chills, dizziness, difficulty of breathing, abdominal pains, and chest, fever, and redness or severe pain at the position of the biopsy [7–10]. Different noninvasive methods are used to reduce unnecessary liver biopsy cases and to observe FLD, mainly imaging techniques, such as ultrasound imaging analysis.

Table 1. Main types of diffused liver diseases and ultrasound findings.

Diseases	Causes	Ultrasound Findings
Fatty liver	Drug misuse, contaminants, metabolic illness, and obesity	Fine parenchymal texture, decreased number of vessels, hepatomegaly, and increased echogenicity
Hepatitis	Infections from viruses/bacteria or parasites.	Diffusely decreased echogenicity and hepatomegaly
Fibrosis	Hepatic venous obstruction, chronic hepatitis, metabolic disorder, prolonged cholestasis, and immune disorder	Healthy appearance of liver, a slight increase in echogenicity, and coarse echo-texture
Cirrhosis	Cystic fibrosis, hepatitis, Wilson’s disease, alpha 1-antitrypsin deficiency, and immune disorder	Shrunken liver, rounded contours, small right lobe with enlarged left and caudate lobes, (volume redistribution), regenerative nodules, and nodularity resulted in portal hypertension manifestations of surface irregularity. Decreased number of vessels.

Ultrasound is preferred by radiologists because it is nonexpensive, noninvasive, easy to operate, and radiation-free. In addition, it provides higher average specificity and sensitivity for detecting fatty liver when compared to other kinds of noninvasive imaging techniques such as (1) Magnetic Resonance (MR) imaging and (2) Computed Tomography (CT). CT is limited by the standardization required for the different scanners and the inter-observer variability. In radiomics [11,12], the standardization of feature extraction methodology is significant for second and higher-order texture features. Furthermore, MR techniques can be technically challenging. A functional MR of the liver diagnosis requires stability adequate for the elimination of patient motion [13–16]; a brief description of these diagnosis approaches is shown in Table 2.

One of the major limitations of using ultrasound is the low quality of the acquired images compared to those of MRI and CT. This means that the classification task is extremely difficult and is one of the challenges addressed in this research.

One method to reduce the limitations of an ultrasound is to improve a Computer-Aided Diagnosis (CAD) system. CAD offers a promising solution to reduce variation in colonoscopy performance [17]. Many of the CAD systems have been developed using

medical liver images for the diagnosis of liver diseases [18,19]. The usage of a CAD method reduces the user’s intervention and helps experts and physicians to detect FLD through analyzing ultrasound images.

Table 2. Invasive and noninvasive test methodology for evaluation of FLD overview.

Diagnosis Methods	Weaknesses and Drawbacks of These Methods	Drawbacks of Those Methods
Liver Biopsy	Examination with prognostic value. Links with the level of liver injury.	It is a technique of invasiveness. Complications such as bleeding and discomfort are likely. Operator dependent.
Blood tests	The leading supporter in the assessment of essential liver function. High sensitivity with improved standards of ALT and AST.	Low specificity. No relationship with the level of diffused liver tissue injury.
MRI	Possibility of analysis of spectroscopy. Proper quantification of the fat content of the human liver.	The high expense of the test. The fat quantification mistakes (or inaccuracies) in the presence of high iron concentration. Unsuitable for patients with planted electronic devices, for example, pacemakers.
CT	Characterize fatty or (steatosis) by the lower liver intensity. Quantitative measurement.	Low sensitivity for early-stage fatty (or steatosis). Use of ionizing radiation. Interequipment variability.
Ultrasound	Advised for initial diagnosis. The high specificity of fat. Accumulation is greater than 33%. Effective, low cost, and noninvasive.	Inappropriate for cases with high Body Mass Index (BMI). Intraoperator variability. Operator dependent.

The CAD introduced by Yeh et al. [20], developed a procedure to make nonsteatosis (healthy liver) distinguished. Nonsteatosis and steatosis (fatty) specials of the liver are imaged by ultrasonography of high frequency. The authors retrieved and used two characteristics, Support Vector Machine (SVM), as a classifier to obtain an accuracy of up to 90%. A CAD system was developed by Ribeiro et al. [21] for classifying steatosis and nonsteatosis using Radio Frequency (RF), the signal made by the ultrasound examination was employed to extract only two images. The first one is a speckle-only image, and the second is a despeckled image with descriptions and anatomical characteristics. The intensity features were calculated from the despeckled image and the speckle image, associated with two texture features extracted. The classification process was performed on two categories, ten steatosis liver images and ten nonsteatosis ultrasonic liver images; the Bayes classifier was used in this study and obtained an accuracy of 95%.

Mittal et al. implement the CAD system in [22], which specialists combined to analyze and diagnose liver focal lesions from 2D-mode ultrasound images. The authors used four different types of focal liver lesions and associated them with the normal human liver. In the ultrasound image, the noise was decreased by filtration, and then they divided the ROIs into 800 segmented sections. Afterward, based on the texture, near 208 texture-based features were extracted from separate ROI. The achieved accuracy of the use of the

ANN approach was about 86%. Acharya et al. [23] suggested a classification manner to discriminate steatosis and a normal human liver. In this study, the authors extracted a combination of image texture features from the diffused liver. Applying this classification technique, the authors obtained an accuracy of about 93%.

Ribeiro et al. proposed a CAD system in [24] for FLD analysis and classification. In total, 36 features were extracted from each selected ROI from the ultrasound image. Then, based on three different classifiers: k-Nearest Neighbor (k-NN), Bayes, and Support Vector Machine (SVM), the obtained accuracy was recorded at 85.71%. Li et al. [25], utilizing an SVM classifier based on liver ultrasound images. The extracted features were from GLCM, Near-Far-Field Greyscale Ratio (NFFGR), and Neighborhood Grey-Tone Difference Matrix (NGTDM). As a consequence of using a previous technique, the total accuracy recorded was 90.55%. Singh et al. [19] proposed a technique based on the fusion information for the hepatic classification by operating an ultrasonic image texture examination. Based on texture examination, a set of texture features are applied in the classification technique. A combination of the best-selected features associated with their weights is suggested. The total accuracy of this technique was 95%.

The common phases of the CAD system based on feature extraction and classification stage were [6]: (1) feature extraction phase, numerous texture features were selected and extracted using the desired and significant features from the ultrasound images of the human liver tissues such as entropy [6], (GLCM) [18,19,26–29], Grey Level Run Length Matrix (GLRLM) [18], FOS [18,19,30], Grey Level Difference Statistics (GLDS) [19,31], Fourier Analysis (FA) [19,27,28], and Statistical Feature Matrix (SEM) [19,27]; (2) Classification stage: many classifiers are proposed in the classification phase, for example, k-NN [27,32], Naive Bayes (NB) [28], Decision Tree (DT) [29,30], AdaBoost [31], Random Forest (RF) [33,34], Fuzzy [35,36] (SVM) [32,37–39], Multilayered Perceptron (MLP) [29,40], Probabilistic Neural Network (PNN) [41], Quadratic Discriminant Analysis (QDA), and Linear Discriminant Analysis (LDA) [6]. The most important purpose of this study is to achieve high recognition accuracy to discriminate between fatty/normal liver.

Unlike the classical machine learning techniques that are used in this study, deep learning was proposed in [42]. Deep learning [43,44] was not feasible to apply in our research work due to the limitation of the dataset.

In our proposed work, there are four main contributions. Firstly, the ultrasound liver images were classified as fatty or normal without the segmentation stage. Secondly, the available dataset in previous works was insufficient compared to our proposed work. Thirdly, decreasing the total number of extracted features to only 26 features turned out to have low computational complexity. Fourthly, the achieved recognition accuracy of the voting-based classifier was better than other classifiers.

The current paper is organized as follows. First, the technique of image acquisition used is described briefly in Section 2, and then Section 3 sets out the proposed work. After that, the experimental results and discussion are described in Section 4. As a final point, the conclusion is set out in Section 5.

3. Materials and Methods

3.1. Image Acquisition

In the current paper, GE Logiq p5 [45] equipment was used for image acquisition. Elroowad Radiography Center, Menouf City, Egypt supplied us with images to be used in this study, by three professional medical radiologists. The transmitting frequency of the ultrasound was (2 to 3) MHz with a convex probe. The resolution of the acquired color image was 684×552 pixels. There were 300 images; one image was acquired from each patient. An experienced radiologist determined the ROI. Corresponding to the decisions of the three experienced radiologists, 155 US images were manually considered as normal liver, and 145 images as fatty liver. This research work focuses on normal/fatty liver images. Figure 1 shows one of the normal and fatty images.

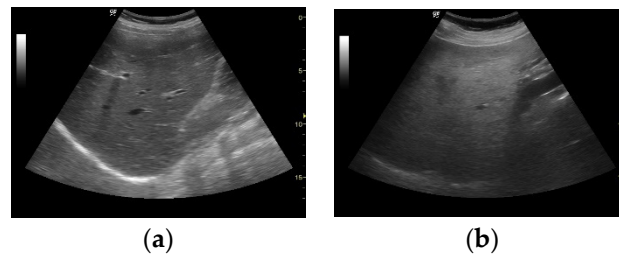


Figure 1. An acquired image from an ultrasound scan machine (a) normal liver and (b) fatty liver.

3.2. Methodology

The main objectives of the present CAD system were 1- To analyze the consequence of a dynamic size of ROI extracted from each ultrasound liver image; 2-To categorize the USA liver images as fatty or normal without the segmentation stage, a voting-based classifier was applied. In this research work, multiple ROIs (nine ROIs) were selected within the liver tissue. This was also automatically determined by the Genetic Algorithm (GA). GA is an adaptive investigative search algorithm [41]. In GA, firstly, an initial population was created. The population consisted of 100 chromosomes. Separately, a chromosome was composed of concatenated thresholds or candidate solutions. The chromosome construction is shown in Figure 2. Secondly, each pair of parent chromosomes was carefully chosen, and then the crossover process was performed at the random crossover point. Thirdly, the mutation operation was executed on every chromosome at a random point. Then, the offspring was generated. Finally, an optimization using an objective function was performed for offspring and the parent chromosomes.

<i>F1 threshold</i>
<i>F2 threshold</i>
⋮
<i>F26 threshold</i>
<i>voting threshold</i>
<i>ROI rows</i>
<i>ROI columns</i>
<i>No. of ROIs</i>

Figure 2. The chromosome structure, note: F1→Feature1, etc.

The objective function was used to exploit the accurately classified US images or to minimize the number of wrongly classified images. The fitness function was reciprocal of the Penalty Value (PV), or precisely the number of incorrectly categorized images. Ultimately, the fitness function was the number of correct categorized images.

The position was initially determined by three experienced physicians. As a consequence of labeling ROIs, the fixed positions were then used for newly acquired images. To make the process faster, only ROIs in the selected images were converted from RGB to a grey level [46], according to the following equation:

$$I = 0.2989 * R + 0.5870 * G + 0.1140 * B \quad (1)$$

where I is a transformed image; then, the 26 features of each ROI were extracted, as in Figure 3. Finally, the voting-based classifier was used to categorize the kind of liver tissue normal/fatty [46]. In a Voting-based classifier, the key concept was to perform multi-independent Extreme Learning Machine (ELM) training in place of one single ELM training, and then a final decision was taken depending on the majority voting method [47].

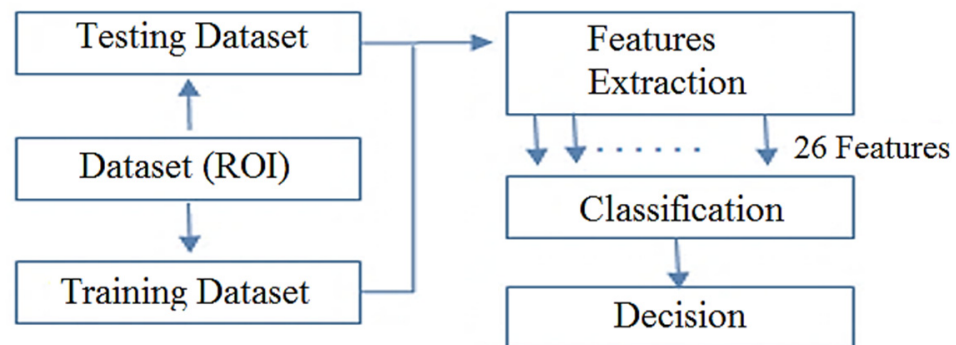


Figure 3. General block diagram of the work proposed.

3.2.1. Feature Extraction

Twenty-six texture features were then extracted from the ultrasonic images of each selected ROI of human liver tissues such as: (A)-FOS which include: (1) Mean, (2) Skewness, (3) Variance, and (4) Kurtosis; (B)-GLCM including (1) Standard deviations, (3) Contrast, (4) Mean, (5) Autocorrelation, (6) Dissimilarity energy, (7) Correlation, (8) Cluster shade, (9) Cluster Prominence, (10) Information measure of correlation, (11) Sum average, (12) Difference variance, (13) Entropy, (14) Sum variance, (15) Sum-of-squares, (16) Sum entropy, (17) maximum probability, (18) Inverse Difference Normalized, (19) Difference entropy, (20) Homogeneity, and (21) Inverse difference moment normalized. These texture features were extracted as in [16].

3.2.2. Classification

For all selected “ROIs,” there were 26 decisions made. This process was repeated for all other ROIs. The number of decisions made for the normal tissue were counted accordingly. Then, this count was compared to a specific threshold, i.e., the voting threshold, as a consequence of the number of ROIs categorized as fatty liver to the number of ROIs categorized as normal liver, a voting-based classifier was used to identify the class of the liver type. The final vote was “normal liver” if the count was greater than the threshold for voting. Otherwise “fatty liver” as the final decision, as shown below in Algorithm 1. Furthermore, to diagnose diffuse liver disease in an accurate manner, dynamic-sized ROIs (row \times column) were proposed. In this study, to prevent manually selected threshold parameters; the GA was used.

Figure 4 shows the general process and the training and the testing phases of the dataset for optimizing a grey ROI selection by using the GA. In the training phase stage, each image of the normal/fatty liver in the training set was employed for the planned work. Then, the thresholds and parameters were automatically selected and optimized by GA, such that this image was identified as a normal or fatty item, respectively. In the testing part, a whole image of the testing set was utilized in the suggested work. Then, according to the voting function, liver tissue was classified as normal/fatty liver.

Algorithm 1: Optimization of the number of ROIs, ROI size selection, and voting threshold

```

1. For iteration number = 1, 2, 3, ... . . . , number of iteration do
2. For every chromosome do
    Number of incorrectly classified images = 0
    For every training image do
        voting = 0
        For every ROI of size,  $m \times n$  do
            Convert ROI into gray level using the equation:
                 $I = 0.2989 * R + 0.5870 * G + 0.1140 * B$ 
            Compute all 26 features
        End for
        If voting > voting_threshold
            If training image = abnormal
                Number of incorrectly classified image +1 →
                Number of incorrectly classified image
            End if
        Else
            If training image = normal
                Number of incorrectly classified image +1 →
                Number of incorrectly classified image
            End if
        End if
    End for
    Assign fitness score to the chromosome
End for
3. For every testing image do
    voting = 0
    For every ROI do
        Convert ROI into gray level
        Compute all 26 features
    End for
    If voting > voting_threshold
        Liver case = normal
    Else
        Liver case = Abnormal
    End if
End for

```

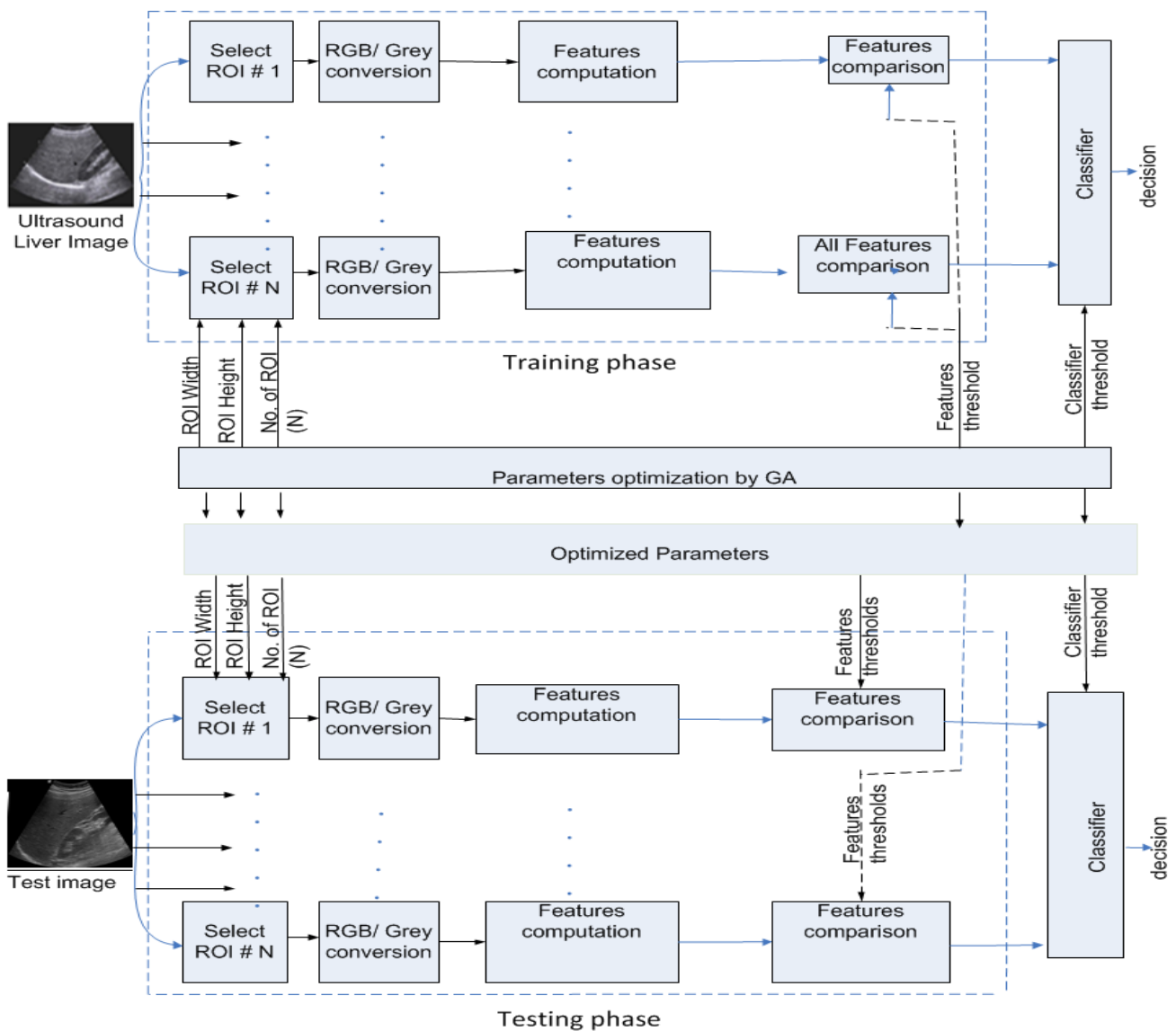


Figure 4. Elevating parameters using a GA and overall process, note: #→Number.

4. Results

This study developed a Computer-Aided Diagnosis technique using the Genetic Algorithm and machine learning algorithms (supervised learning), for the classification of liver skins as being fatty or natural, based on obtaining ultrasound image features and a voting-based classifier, based on a combination of 26 features.

4.1. Genetic Algorithm

In this study, 300 images were collected from 300 patients of 155 normal and 145 fatty cases. Every acquired image was processed as presented in Figure 5a; then, it was converted to a grey level image (by using Equation (1)), as shown in Figure 5b. As a consequence, a number of ROIs were carefully chosen within the liver tissue from the training set, as shown in Figure 5c. These suggested regions covered the tissue of the liver, as indicated by the specialized physician and experts.

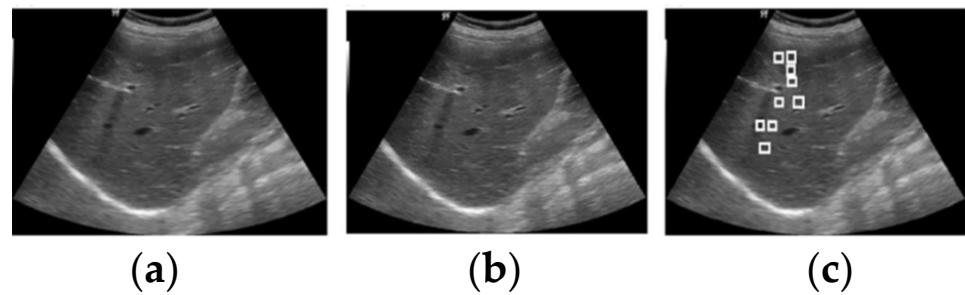


Figure 5. (a) Ultrasonic image (Original). (b) The transformed US image by using Equation (1). (c) The selected grey ROIs.

The collected data set was categorized into testing and training sets. The training images included 110 fatty images and 120 normal images. Whereas, the testing images involved 35 fatty images and 35 natural images.

The generation increased as “false negatives” or the number of wrongly classified US images decreased in the following figure “Best: 2” meant that only two images in the training set were mistakenly categorized, as presented in Figure 6.

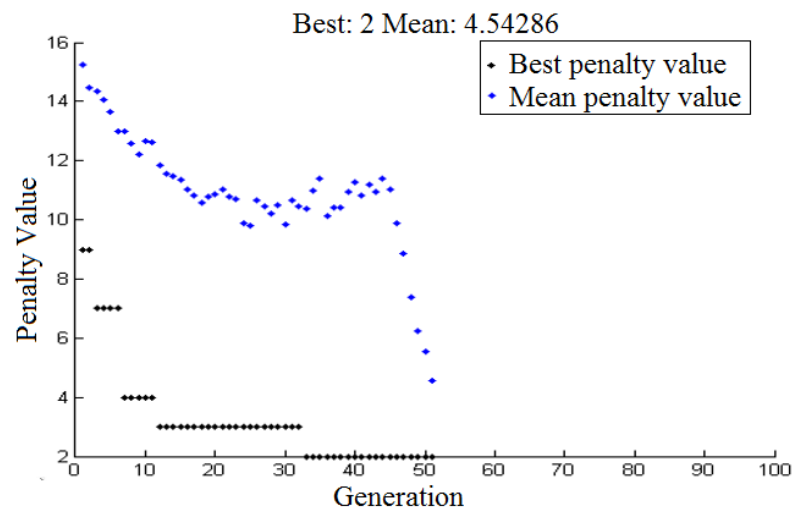


Figure 6. The change in penalty values due to generation numbers.

Table 3 exhibits the number of US images that were classified correctly or incorrectly. It also presents the evaluated classification percentages in the case of the training and testing images.

Table 3. Classification percentages of the liver images.

(a) Classification percentages for the training images.			
Case	True Images	False Images	Total
Training images	228	2	230
Accuracy	99.13%	0.87%	100%
(b) Classification calculations for the testing US images.			
Case	True Images	False Images	Total
Testing images	67	3	70
Accuracy	95.71%	4.29%	100%

4.2. Performance Evaluation Metrics

In our case, the number of testing images was 70 (35 + 35) for the two groups (fatty and natural). When no disease was found, True Negatives (TN) were observed, and the test was

negative, while it was classified as false positive (FP) if the test was positive. Instead, if the disease was present, a positive or negative test indicated the observations were classified as True Positive (TP) or False Negative (FN) situations, respectively [17,48,49]. Subsequent performance measures are displayed in Table 4.

Table 4. The values of TN, TP, FP, and FN.

	Case: Normal/Fatty (70 Test Images) 35 Normal and 35 Fatty
TP	33 (94.28%)
TN	34 (97.14%)
FP	2 (5.71%)
FN	1 (2.85%)
Total	70

Table 5 presents the robust widely used performance measures: *sensitivity*, *accuracy*, *precision*, *specificity*, and *F1-score*. *Accuracy* is an intuitive measure of *accuracy* and is simply the ratio of properly expected observations to total observations. *Precision* is a calculation of correctly expected real observations to total predicted real observations. The *sensitivity* (recall) is a ratio of the relevant instances that were regained. *Specificity* is a proportion of healthy persons who were correctly reported as not having the illness. Finally, the *F1-Score* is the average of sensitivity and precision. Consequently, the aforementioned score takes both *FP* and *FN* into account [48,49] These performance metrics are known by:

$$Accuracy = \frac{(TN + TP)}{(TN + TP + FN + FP)} \quad (2)$$

$$Precision = \frac{TP}{(FP + TP)} \quad (3)$$

$$Sensitivity = \frac{TP}{(FN + TP)} \quad (4)$$

$$Specificity = \frac{TN}{(FP + TN)} \quad (5)$$

$$F1_{-}measure = 2 * \frac{(Sensitivity * Precision)}{(Sensitivity + Precision)} \quad (6)$$

Table 5. Evaluation of some performance metrics.

Performance Metrics	Percentage
<i>Accuracy</i>	95.71%
<i>Precision</i>	94.28%
<i>Sensitivity</i>	97.05%
<i>Specificity</i>	94.44%
<i>F1-score</i>	95.64%

Table 6 introduces a comparison of the recognition rate of our proposed technique with that in [18,23,26,50]. Our proposed technique produced more accurate results than those in the referred references. The suggested method achieved better accuracy compared to other research. It should be noted that the work by other researchers used an ultrasound imaging system, which was better than the proposed image acquisition system. Our acquisition system was a very popular product in the field of medical equipment, because it was so inexpensive compared to other acquisition systems. The range of the transmitting frequency

of the ultrasound in our device was the same with other devices. The resolution of 684×552 pixels in our device was lower than the resolution of other devices, e.g., 767×572 pixels and 1024×1024 pixels. Moreover, the research work by [18,23,26,50] used a greater number of extracted features, which required high computation complexity. The use of a smaller number of features allowed us to avoid the use of GPU as in [51,52].

Table 6. Comparison between the suggested method and other systems.

Authors	Classes (No. of Patients)	Features/Classifier	Performance
Acharya et al. [23]	42 Natural, 58 Fatty	Texture, wavelet transform, and DT/HOS and FSC	An accuracy: 93.3%
Andrade et al. [18]	Natural, Fatty. 177 echographic ultrasonic images were acquired from 36 patients	GLRLM, law’s texture energy, FOS, GLCM, and fractal dimension/ANN, SVM&KNN	76.92% 79.77% 74.05% respectively
Kalyan et al. [26]	Natural (30), Fatty (10), Cirrhotic (10), Hep. (10)	GLRLM, Invariant moments, Intensity histogram, GLCM/BPNN	92.5%
Santos et al. [50]	Natural (68), Fatty (52)	FOS, GLCM, GLRLM, Gabor filter, Laws’ filter, lacunarity, fractal dimension, hepatorenal coefficient, attenuation/ ANN, SVM, k-NN, Bayes, DT	classifiers fusion:79%
Sharma et al. [16]	45 Natural, 45 Fatty	FOS, GLCM, GLRLM, Law’s TEM, FPS, Fractal	Accuracy: 95.55%,
The current work	Natural (155), Fatty (145)	26 features/Voting Function	Accuracy: 95.71%

4.3. Machine Learning Algorithms

Supervised learning algorithms were employed in this investigation to classify the liver tissues into fatty and normal using the same data set that was used before in the genetic algorithm. Several algorithms were applied to construct the classifier model, but we reported the greatest classifier decision tree (J48), that given the high accuracy, it achieved accuracy reaching up to 93.12%, according to the main parameters, the Kappa statistic was 0.85, mean absolute error was 0.069, root mean squared error was 0.26, relative absolute error was 0.1451, and root relative squared error was 0.5383.

This classifier was tested using the cross-validation (10 folds) method; in this method, the dataset was divided randomly into 10 folds, each fold was held out once to test the classifier, and the classifier was trained on the remaining (10-1) to build the classifier as shown in Figure 7 [44]. Each fold represented one iteration, in each iteration, the accuracy of the model was calculated, and the overall accuracy was calculated using the mean; this method was the best to evaluate the performance of the model, based on different measures mainly: TP rate, FP rate, Precision, recall, and F1-measure as shown in Table 7 and also presented in Figure 8. The Experimental Results were developed and evaluated using WEKA software version 3.6.11.

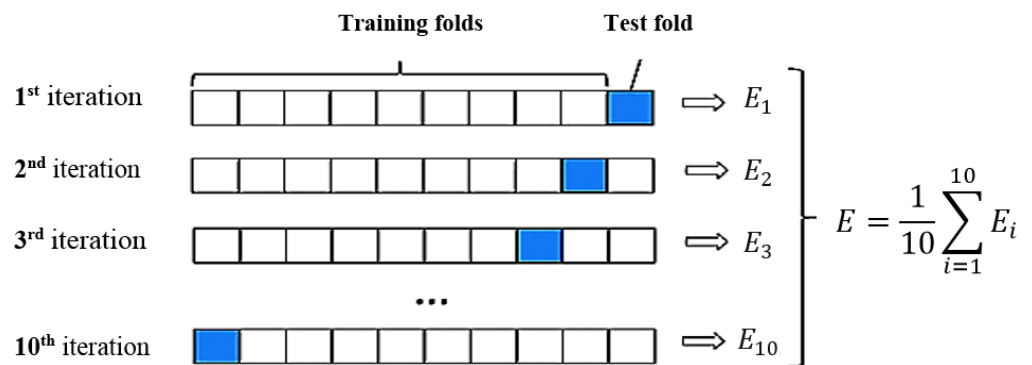


Figure 7. Ten-fold cross-validation method.

Table 7. Precision, Recall, and F1-Measure for J48 algorithm.

Decision Tree (J48)						
Class	TP Rate	FP Rate	Precision	Recall	F-Measure	ROC Area
Fatty	0.944	0.091	0.944	0.944	0.944	0.927
Normal	0.909	0.056	0.909	0.909	0.909	0.927
AVG	0.931	0.077	0.931	0.931	0.931	0.927

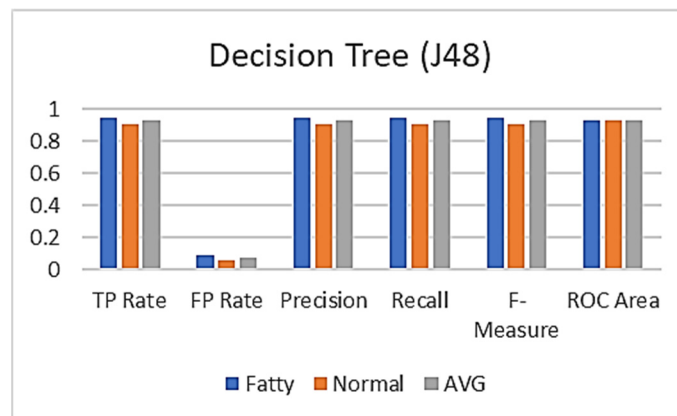


Figure 8. Precision, Recall, and F1-Measure for J48 algorithm.

5. Conclusions

Early diagnosis of FLD is important to avoid advanced stages. Due to its low cost and availability, radiologists commonly use US imaging. However, it has problems in detecting this disease due to its low quality. The current study provided a technique to accurately distinguish between fatty/normal livers using ultrasound liver images. Ultrasound, as a noninvasive method, was known for diagnosing diffused liver diseases. In this work, multi ROIs were selected to reduce the required computations. From each ROI, 26 features were extracted. The acquired image of fatty tissue was characterized by bright echogenicity with high contrast and high variance. All thresholds and parameters were automatically selected via GA. The final result depended on the number of normal/fatty ROIs. The obtained TP was 94.28%, TN was 97.14%, FP was 5.71%, and FN was 2.85%. The achieved precision was 94.28%, sensitivity was 97.05%, specificity was 94.44%, and F1-score was 95.64%. The proposed work provided a high recognition percentage of 95.71% compared to previous research work, which achieved lower recognition accuracies 76.92%, 79.77%, 74.05%, 92.5%, 79%, 95.55%, and 93.3%. Moreover, it should be declared that the number of extracted features in the current study was lower than that found in the literature, which significantly achieved lower computational time in classifying the liver.

The limitation of our technique is a deficiency of available databases. Moreover, the low quality of acquisition ultrasound devices leads to a requirement for improved methods including more efficient functionality without degrading the ultrasound image content.

As future research, the accuracy of recognition of the proposed method could be improved by reducing the rate of False-Negative (FN) cases to allow us to better distinguish between closely resembling diseases. Future work would be on increasing the size of patient datasets to improve and increase the classification accuracy of the system and generalizing the proposed method to deal with US images. Class imbalance is also challenging. For instance, liver cirrhosis is usually so limited compared to other classes; e.g., liver steatosis, liver cancer, and liver fibrosis. Additionally, more specific classes can be added, e.g., stages of fibrosis; F1, F2, F3, and F4. It should be mentioned that these classes of fibrosis are so difficult to be recognized by specialists radiologist. This is because some details are invisible to human eyes.

Before CAD technology and artificial intelligence are incorporated into routine clinical practice, several challenges must be overcome. For clinical use, if there are concerns about unreliable predictions, a CAD system must be able to justify its analysis.

The possibility that CAD will replace completely human decision making is unlikely in the meantime. Should CAD technology be used as the strategy of resect-and-discard for benign tumors then photo-documentation with high-resolution images marked with CAD decisions will be needed for medical-legal reasons.

Author Contributions: Conceptualization, A.G., H.A.Y., A.M.H. and A.H.; methodology, A.G., A.H., A.M.H. and H.A.Y.; software, A.G. and A.H.; validation, A.G., A.H., H.A.Y. and H.M.A.; investigation, A.G., A.H. and H.A.Y.; resources, A.G.; data curation, A.G., A.M.H. and H.A.Y.; writing—original draft preparation, A.G., A.H.; writing—review and editing, A.G., A.M.H. and H.A.Y.; supervision, A.H. and H.A.Y. All authors have read and agreed to the published version of the manuscript.

Funding: This research received no external funding.

Institutional Review Board Statement: Not applicable.

Informed Consent Statement: Not applicable.

Data Availability Statement: Data sharing is not applicable.

Acknowledgments: The authors are grateful to Elroowad Radiography Center (Menouf City, Egypt), especially to Ahmed F. Yonis for providing the USA images used in this investigation, and for supportive discussions.

Conflicts of Interest: The authors declare no conflict of interest.

References

1. Marcellin, P.; Kutala, B.K. Liver diseases: A major, neglected global public health problem requiring urgent actions and large-scale screening. *Liver Int.* **2018**, *38*, 2–6. [[CrossRef](#)] [[PubMed](#)]
2. Cotter, T.G.; Rinella, M. Nonalcoholic fatty liver disease 2020: The state of the disease. *Gastroenterology* **2020**, *158*, 1851–1864. [[CrossRef](#)] [[PubMed](#)]
3. Stepanova, M.; De Avila, L.; Afendy, M.; Younossi, I.; Pham, H.; Cable, R.; Younossi, Z.M. Direct and indirect economic burden of chronic liver disease in the United States. *Clin. Gastroenterol. Hepatol.* **2017**, *15*, 759–766. [[CrossRef](#)]
4. Kelly, N.; Wattacheril, J. Nonalcoholic fatty liver disease: Evidence-based management and early recognition of nonalcoholic steatohepatitis. *J. Nurse Pract.* **2019**, *15*, 622–626. [[CrossRef](#)]
5. Duseja, A. Nonalcoholic fatty liver disease in India—a lot done, yet more required! *Indian J. Gastroenterol.* **2010**, *29*, 217–225. [[CrossRef](#)] [[PubMed](#)]
6. Acharya, U.R.; Raghavendra, U.; Fujita, H.; Hagiwara, Y.; Koh, J.E.; Hong, T.J.; Ng, K.H. Automated characterization of fatty liver disease and cirrhosis using curvelet transform and entropy features extracted from ultrasound images. *Comput. Biol. Med.* **2016**, *79*, 250–258. [[CrossRef](#)] [[PubMed](#)]
7. Sumida, Y.; Nakajima, A.; Itoh, Y. Limitations of liver biopsy and non-invasive diagnostic tests for the diagnosis of nonalcoholic fatty liver disease/nonalcoholic steatohepatitis. *World J. Gastroenterol. WJG* **2014**, *20*, 475. [[CrossRef](#)] [[PubMed](#)]
8. Nalbantoglu, I.; Brunt, E.M. Role of liver biopsy in nonalcoholic fatty liver disease. *World J. Gastroenterol. WJG* **2014**, *20*, 9026.
9. Tapper, E.B.; Lok, A.S.F. Use of liver imaging and biopsy in clinical practice. *N. Engl. J. Med.* **2017**, *377*, 756–768. [[CrossRef](#)]
10. Castera, L. Non-invasive assessment of liver fibrosis in chronic hepatitis C. *Hepatol. Int.* **2011**, *5*, 625–634. [[CrossRef](#)]

11. Sanchez, L.E.; Rundo, L.; Gill, A.B.; Hoare, M.; Serrao, E.M.; Sala, E. Robustness of radiomic features in CT images with different slice thickness, comparing liver tumour and muscle. *Sci. Rep.* **2021**, *11*, 8262. [[CrossRef](#)]
12. Shafiq-ul-Hassan, M.; Latifi, K.; Zhang, G.; Ullah, G.; Gillies, R.; Moros, E. Voxel size and gray level normalization of CT radiomic features in lung cancer. *Sci. Rep.* **2018**, *8*, 8262. [[CrossRef](#)]
13. Van Beers, B.E.; Daire, J.L.; Garteiser, P. New imaging techniques for liver diseases. *J. Hepatol.* **2015**, *62*, 690–700. [[CrossRef](#)]
14. Shahbazi, H.; Taban, M.R.; Abouei, J. A new approach to design sensing matrix based on the sparsity constant with applications to computed tomography. *IEEE Access* **2019**, *7*, 175396–175410. [[CrossRef](#)]
15. Zhang, Y.D.; Zhang, Y.; Dong, Z.; Yuan, T.F.; Han, L.; Yang, M.; Lu, H. IEEE Access Special Section Editorial: Advanced Signal Processing Methods In Medical Imaging. *IEEE Access* **2018**, *6*, 61812–61818. [[CrossRef](#)]
16. Sharma, V.; Juglan, K.C. Automated classification of fatty and normal liver ultrasound images based on mutual information feature selection. *IRBM* **2018**, *39*, 313–323. [[CrossRef](#)]
17. Ahmad, O.F.; Soares, A.S.; Mazomenos, E.; Brandao, P.; Vega, R.; Seward, E.; Lovat, L.B. Artificial intelligence and computer-aided diagnosis in colonoscopy: Current evidence and future directions. *Lancet Gastroenterol. Hepatol.* **2019**, *4*, 71–80. [[CrossRef](#)]
18. Andrade, A.; Silva, J.S.; Santos, J.; Belo-Soares, P. Classifier approaches for liver steatosis using ultrasound images. *Procedia Technol.* **2012**, *5*, 763–770. [[CrossRef](#)]
19. Singh, M.; Singh, S.; Gupta, S. An information fusion based method for liver classification using texture analysis of ultrasound images. *Inf. Fusion* **2014**, *19*, 91–96. [[CrossRef](#)]
20. Yeh, W.C.; Jeng, Y.M.; Li, C.H.; Lee, P.H.; Li, P.C. Liver steatosis classification using high-frequency ultrasound. *Ultrasound Med. Biol.* **2005**, *31*, 599–605. [[CrossRef](#)]
21. Ribeiro, R.; Sanches, J. Fatty liver characterization and classification by ultrasound. In *Iberian Conference on Pattern Recognition and Image Analysis*; Springer: Berlin/Heidelberg, Germany, 2009; pp. 354–361.
22. Mittal, D.; Kumar, V.; Saxena, S.C.; Khandelwal, N.; Kalra, N. Neural network based focal liver lesion diagnosis using ultrasound images. *Comput. Med. Imaging Gr.* **2011**, *35*, 315–323. [[CrossRef](#)]
23. Acharya, U.R.; Sree, S.V.; Ribeiro, R.; Krishnamurthi, G.; Marinho, R.T.; Sanches, J.; Suri, J.S. Data mining framework for fatty liver disease classification in ultrasound: A hybrid feature extraction paradigm. *Med. Phys.* **2012**, *39*, 4255–4264. [[CrossRef](#)]
24. Ribeiro, R.; Marinho, R.T.; Sanches, J.M. Global and local detection of liver steatosis from ultrasound. In Proceedings of the 2012 Annual International Conference of the IEEE Engineering in Medicine and Biology Society, San Diego, CA, USA, 28 August–1 September 2012; IEEE: Piscataway, NY, USA, 2012; pp. 6547–6550.
25. Li, G.; Luo, Y.; Deng, W.; Xu, X.; Liu, A.; Song, E. Computer aided diagnosis of fatty liver ultrasonic images based on support vector machine. In Proceedings of the 2008 30th Annual International Conference of the IEEE Engineering in Medicine and Biology Society, Vancouver, BC, Canada, 20–24 August 2008; IEEE: Piscataway, NY, USA, 2008; pp. 4768–4771.
26. Kalyan, K.; Jakhia, B.; Lele, R.D.; Joshi, M.; Chowdhary, A. Artificial neural network application in the diagnosis of disease conditions with liver ultrasound images. *Adv. Bioinform.* **2014**, *2014*, 708279. [[CrossRef](#)]
27. Rong, H.; Wang, H.M.; Liu, J.; Xian, M. Privacy-preserving k-nearest neighbor computation in multiple cloud environments. *IEEE Access* **2016**, *4*, 9589–9603. [[CrossRef](#)]
28. Meejaroen, K.; Chaweechan, C.; Khodsiri, W.; Khu-Smith, V.; Watchareeruetai, U.; Sornmagura, P.; Kittiyakara, T. Detection of fibrosis in liver biopsy images by using Bayesian classifier. In Proceedings of the 2015 7th International Conference on Knowledge and Smart Technology (KST), Chon Buri, Thailand, 28–31 January 2015; IEEE: Piscataway, NY, USA, 2015; pp. 184–189.
29. Abdelaal, H.M.; Elemetry, B.R.; Youness, H.A. Classification of hadith according to its content based on supervised learning algorithms. *IEEE Access* **2019**, *7*, 152379–152387. [[CrossRef](#)]
30. He, Q.; Xu, Z.; Li, S.; Li, R.; Zhang, S.; Wang, N.; Chen, W. Novel entropy and rotation forest-based credal decision tree classifier for landslide susceptibility modeling. *Entropy* **2019**, *21*, 106. [[CrossRef](#)]
31. Ibrahim, A.; Tharwat, A.; Gaber, T.; Hassanien, A.E. Optimized superpixel and AdaBoost classifier for human thermal face recognition. *Signal Image Video Processing* **2018**, *12*, 711–719. [[CrossRef](#)]
32. Di Ruberto, C.; Loddo, A.; Putzu, L. A multiple classifier learning by sampling system for white blood cells segmentation. In Proceedings of the International Conference on Computer Analysis of Images and Patterns, Valletta, Malta, 2–4 September 2015; Springer: Cham, Switzerland, 2015; pp. 415–425.
33. Chlebus, G.; Meine, H.; Moltz, J.H.; Schenk, A. Neural network-based automatic liver tumor segmentation with random forest-based candidate filtering. *arXiv* **2017**, arXiv:1706.00842.
34. Wu, C.C.; Yeh, W.C.; Hsu, W.D.; Islam, M.M.; Nguyen, P.A.A.; Poly, T.N.; Wang, Y.C.; Yang, H.C.; Li, Y.C.J. Prediction of fatty liver disease using machine learning algorithms. *Comput. Methods Programs Biomed.* **2019**, *170*, 23–29. [[CrossRef](#)]
35. Das, A.; Das, P.; Panda, S.S.; Sabut, S. Adaptive fuzzy clustering-based texture analysis for classifying liver cancer in abdominal CT images. *Int. J. Comput. Biol. Drug Des.* **2018**, *11*, 192–208. [[CrossRef](#)]
36. Ma, J.; Li, Y.; Wu, Y.; Zhang, M.; He, J.; Qiu, Y.; Yang, X. Automatic Liver Tumor Segmentation Based on Random Forest and Fuzzy Clustering. In *International Conference on Sensing and Imaging*; Springer: Cham, Switzerland, 2017; pp. 403–410.
37. Muthuswamy, J. Extraction and Classification of Liver Abnormality Based on Neutrosophic and SVM Classifier. In *Progress in Advanced Computing and Intelligent Engineering*; Springer: Singapore, 2019; pp. 269–279.
38. Bhardwaj, R.; Mehta, R.; Ramani, P. A Comparative Study of Classification Algorithms for Predicting Liver Disorders. In *Intelligent Computing Techniques for Smart Energy Systems*; Springer: Singapore, 2020; pp. 753–760.

39. Zhu, Y.; Gao, W.; Guo, Z.; Zhou, Y.; Zhou, Y. Liver tissue classification of en face images by fractal dimension-based support vector machine. *J. Biophotonics* **2020**, *13*, e201960154. [[CrossRef](#)]
40. Cao, Y.; Hu, Z.D.; Liu, X.F.; Deng, A.M.; Hu, C.J. An MLP classifier for prediction of HBV-induced liver cirrhosis using routinely available clinical parameters. *Dis. Markers* **2013**, *35*, 653–660. [[CrossRef](#)]
41. Wu, S.G.; Bao, F.S.; Xu, E.Y.; Wang, Y.X.; Chang, Y.F.; Xiang, Q.L. A leaf recognition algorithm for plant classification using probabilistic neural network. In Proceedings of the 2007 IEEE International Symposium on Signal Processing and Information Technology, Giza, Egypt, 15–18 December 2007; IEEE: Piscataway, NY, USA, 2007; pp. 11–16.
42. Castiglioni, I.; Rundo, L.; Codari, M.; Di Leo, G.; Salvatore, C.; Interlenghi, M.; Sardanelli, F. AI applications to medical images: From machine learning to deep learning. *Phys. Med.* **2021**, *83*, 9–24. [[CrossRef](#)]
43. Riquelme, D.; Akhloufi, M.A. Deep learning for lung cancer nodules detection and classification in CT scans. *AI* **2020**, *1*, 28–67. [[CrossRef](#)]
44. Reddy, D.S.; Bharath, R.; Rajalakshmi, P. A novel computer-aided diagnosis framework using deep learning for classification of fatty liver disease in ultrasound imaging. In Proceedings of the 2018 IEEE 20th International Conference on e-Health Networking, Applications and Services (Healthcom), Ostrava, Czech Republic, 17–20 September 2018; IEEE: Piscataway, NY, USA, 2018; pp. 1–5.
45. GE Healthcare LOGIQ P5 User Manual. Available online: <https://www.manualsdir.com/manuals/254628/ge-healthcare-logiq-p5.html?download> (accessed on 8 January 2021).
46. Gaber, A.; Attiya, G.; Hamdy, A.; Elsayed, T. Recognition of diffuse liver cirrhosis based on image analysis. *Imaging Sci. J.* **2016**, *64*, 152–159. [[CrossRef](#)]
47. Cao, J.; Lin, Z.; Huang, G.B.; Liu, N. Voting based extreme learning machine. *Inf. Sci.* **2012**, *185*, 66–77. [[CrossRef](#)]
48. Abdelaal, H.M.; Ahmed, A.M.; Ghribi, W.; Alansary, H.A.Y. Knowledge Discovery in the Hadith According to the Reliability and Memory of the Reporters Using Machine Learning Techniques. *IEEE Access* **2019**, *7*, 157741–157755. [[CrossRef](#)]
49. Mabrouk, A.G.; Hamdy, A.; Abdelaal, H.M.; Elkattan, A.G.; Elshourbagy, M.M.; Youness, H.A. Automatic Classification Algorithm for Diffused Liver Diseases Based on Ultrasound Images. *IEEE Access* **2021**, *9*, 5760–5768. [[CrossRef](#)]
50. Santos, J.; Silva, J.S.; Santos, A.A.; Belo-Soares, P. Detection of pathologic liver using ultrasound images. *Biomed Signal Process Control.* **2014**, *14*, 248–255. [[CrossRef](#)]
51. Rundo, L.; Tangherloni, A.; Galimberti, S.; Cazzaniga, P.; Woitek, R.; Sala, E.; Nobile, M.S.; Mauri, G. HaraliCU: GPU-powered Haralick feature extraction on medical images exploiting the full dynamics of gray-scale levels. In *International Conference on Parallel Computing Technologies*; Springer: Cham, Switzerland, 2019; pp. 304–318. [[CrossRef](#)]
52. Tsai, H.Y.; Zhang, H.; Hung, C.L.; Min, G. GPU-accelerated features extraction from magnetic resonance images. *IEEE Access* **2017**, *5*, 22634–22646. [[CrossRef](#)]